Electronic Supplementary Material (ESI) for Journal of Materials Chemistry C.

Electronic supporting information available

C_1-symmetric [Ir(C^N^1)(C^N^2)(N^O)]-*tris*-heteroleptic Ir(III)-complexes with horizontal orientation for efficient near-infrared (NIR) polymer light-emitting diodes (PLEDs)

Wentao Li,‡[a] Tiezheng Miao,‡[a] Baowen Wang,[a] Jiaxiang Liu,[a] Xingqiang Lü,[a,*]Guorui Fu,[a,c*] Weixu Feng[b,*] and Wai-Yeung Wong[c,*]

Supporting information

Materials and methods

All reagents were received from Sigma Aldrich and used without further purification. All solvents unless otherwise stated were degassed and stored over 3 Å activated molecular sieves prior to use. All manipulations of air and water sensitive compounds were carried out under dry N_2 using the standard Schlenk line techniques.

Elemental analysis (EA) was performed on a Perkin-Elmer 240C elemental analyzer. Fourier Transform Infrared (FT-IR) spectra were recorded on a Nicolet Nagna-IR 550 spectrophotometer in the region 4000-400 cm^{-1} using KBr pellets. $^1H/^{13}C$ NMR spectra were recorded on a JEOL EX 400 spectrometer with $SiMe_4$ as internal standard in $CDCl_3$ or DMSO-d_6 at room temperature. Electro-spray ionization mass spectrometry (ESI-MS) was performed on a Finnigan LCQ^{DECA} XP HPLC-MS_n mass spectrometer with a mass to charge

(*m/z*) range of 4000 using a standard electro-spray ion source and CH_2Cl_2 as the solvent. Electronic absorption spectra in the UV-visible-NIR region were recorded with a Cary 300 UV spectrophotometer. Visible or NIR emission and excitation spectra were collected by a combined fluorescence lifetime and steady-state spectrometer (FLS-980, Edinburgh) with a 450 W Xe lamp. Excited-state decay times were obtained by the same spectrometer but with a μF900 Xe lamp. The quantum yield (Φ_{PL}) in solution was measured with free-base tetraphenylporphyrin (Φ_r = 0.13 in toluene solution at 298 K) as the standard.[1] The solution was degassed by three freeze-pump-thaw circles. The following equation 1 was used to calculate the quantum yields:

$$\Phi_s = \Phi_r \times [(n_s^2 \times A_r \times I_s)/(n_r^2 \times A_s \times I_r)] \qquad (1)$$

where Φ_s is the quantum yield of the sample, Φ_r is the quantum yield of the reference, n_s is the refractive index of the sample, n_r is the refractive index of the reference, A_s and A_r are the absorbance of the sample and the reference at the wavelength of excitation (355 nm), respectively, and the I_s and I_r are the integrated areas of emission bands of the sample and the reference from 600 to 900 nm, which were recorded by a red photomultiplier tube (PMT) detector. Thermal properties were characterized using thermogravimetric (TG) analyses on a NETZSCH TG 209 instrument under a flow of nitrogen at a heating rate of 10 °C/min.

Synthesis of the C^N[1] ligand Hiqbt (1-(benzo[b]-thiophen-2-yl)-isoquinoline)

The C^N[1] ligand **Hiqbt** was synthesized from the improved Suzuki coupling reaction of 2-chloro-isoquinoline[2] (instead of 2-bromo-isoquinoline[3]) with benzo[*b*]thien-2-yl boronic acid. A mixture of 2-chloro-isoquinoline (0.653 g, 4.0 mmol) and benzo[*b*]thien-2-y boronic acid

(0.713 g, 4.0 mmol) was dissolved into absolute mixed solvents of toluene-EtOH (60 mL; v/v = 2:1) under a N_2 atmosphere. Then an aqueous solution (20 mL) of Na_2CO_3 (2 M) was added, and the mixture was degassed by a N_2 flow. Anhydrous $Pd(PPh_3)_4$ (190 mg, 0.2 mmol; 5 mol%) was added to the reaction mixture which was then heated at 85 °C for 48 h. The complete consumption of reagents was monitored by thin-layer chromatography (Hexane/AcOEt, v/v = 9:1; R_f = 0.25). After cooling to room temperature, the organic phase was washed with brine and extracted with absolute CH_2Cl_2 (3×20 mL) three times. The combined organic phase was dried over anhydrous Na_2SO_4, and further purified with flash-column chromatography on silica gel (Hexane/AcOEt, v/v = 9:1), affording an off-white solid. Yield: 0.762 g (73%). Calcd for $C_{17}H_{11}NS$: C, 78.13; H, 4.24; N, 5.36%. Found: C, 78.05; H, 4.36; N, 5.29%. ^{1}H NMR (400 MHz, DMSO-d_6): δ (ppm) 8.70 (d, 1H, -Py), 8.61 (d, 1H, -Ph), 8.19 (s, 1H, -Th), 8.11 (d, 1H, -Ph), 8.06 (m, 1H, -Ph), 8.02 (m, 1H, -Py), 7.88 (m, 2H, -Ph), 7.81 (m, 1H, -Ph), 7.46 (m, 2H, -Ph).

X-Ray Crystallography

Single crystals for the Ir(III)-complex [Ir(iqbt)(ppy)(pic)] (**1**) or [Ir(iqbt)(ppy)(Br-pic)]·2$CHCl_3$ (**2**·2$CHCl_3$) of suitable dimensions were mounted onto thin glass fibers. All the intensity data were collected on a Bruker APEX-II CCD diffractometer (Mo-Kα radiation and λ = 0.71073 Å) in Φ and ω scan modes. Structures were solved by Direct methods followed by difference Fourier syntheses, and then refined by full-matrix least-squares techniques against F^2 using SHELXTL.[4] All other non-hydrogen atoms were refined with anisotropic thermal parameters. Absorption corrections were applied using SADABS.[5] All hydrogen atoms were placed in

calculated positions and refined isotropically using a riding model. Crystallographic data, relevant atomic distances and bond angles for the C_1-symmetric Ir(III)-complex [Ir(iqbt)(ppy)(pic)] (**1**) and [Ir(iqbt)(ppy)(Br-pic)]·2$CHCl_3$ (**2**·2$CHCl_3$) are presented in **Tables S1-2**, respectively. The CCDC numbers 2080765-2080766 for the C_1-symmetric Ir(III)-complex [Ir(iqbt)(ppy)(pic)] (**1**) and [Ir(iqbt)(ppy)(Br-pic)]·2$CHCl_3$ (**2**·2$CHCl_3$), respectively.

Electronic structure calculations

To gain further insight into the photo-physical and electrochemical characteristics of the Ir(III)-complexes, theoretical studies on their electronic structures were carried out by using density functional theory (DFT) and time-dependent DFT (TD-DFT) methods. Each of their molecular structures was optimized at the ground state (S_0) in the gas phase. DFT calculations were conducted with the popular B3LYP functional theory. The 6-31G (d,p) basis set was applied for C, H, N, O, S and Br atoms, while effective core potentials employed for Ir atom were based on a LanL2DZ basis set.[6-7] The energies of the excited states of the Ir(III)-complex were computed by TD-DFT based on all the ground-state (S_0) geometries. The contributions of fragments to the ‘‘holes’’ and ‘‘electrons’’ and Inter Fragment Charge Transfer (IFCT)[8] in the electronic excitation process were analyzed by the Ros and Schuit method[9] (C-squared population analysis method, SCPA) in the Multiwfn 3.8 program.[10] All calculations were carried out with Gaussian 09, Revision D.01 software package.[11] The electron density diagrams of molecular orbitals were obtained with the ChemOffice 2010 graphics program.

Cyclic voltammetry (CV) measurement

Electro-chemical measurements were made using a Princeton Applied Research model 2273A potentiostat at a scan rate of 100 mV s^{-1}. A conventional three-electrode configuration consisting of a glassy carbon working electrode, a Pt-sheet counter electrode, and a Pt wire reference electrode was used. The supporting electrolyte was 0.1 M tetrabutylammonium tetrafluoroborate ($[Bu_4N]BF_4$) in anhydrous MeCN. Ferrocene was added as a calibrant after each set of measurements, and all potentials reported are quoted with reference to the Fc^+/Fc couple. The oxidation (E_{ox}) and reduction (E_{red}) potentials were used to determine the HOMO and LUMO energy levels using Equations (2) and (3),[12] respectively,

$$E_{HOMO} = -[E_{ox} - E^{1/2,}{}_{ferrocene}] + 4.8 \text{ eV} \qquad (2)$$

$$E_{LUMO} = -[E_{red} - E^{1/2,}{}_{ferrocene}] + 4.8 \text{ eV} \qquad (3)$$

in which, E_{ox} is the recorded onset oxidation potential, and E_{red} is the recorded onset reduction potential using the internal standard ferrocene value of 4.8 eV with respect to the vacuum level. The HOMO and LUMO energy levels for the other materials used were obtained from the literature reference.[13]

Fabrication and testing of the NIR-PLEDs-1-2

Each of the **NIR-PLEDs-1-2** was fabricated on ITO (Indium tin oxide) coated glass substrates with a sheet resistance of 20 Ω per square. Patterned ITO coated glass substrates were washed with acetone, detergent, D. I. water and isopropanol in an ultrasonic bath. After being exposed under oxygen plasma for 20 min, PEDOT:PSS from water solution was spin-

coated (at 4800 rpm) on the substrate followed by drying in a vacuum oven at 130 °C for 30 min, giving a film of 50 nm in thickness. The DCM solution (10 mg/mL) of the mixture of PVK, OXD7 and one of the C_1-symmetric [Ir(C^N^1)(C^N^2)(N^O)]-*tris*-heteroleptic Ir(III)-complexes **1**-**2** as the emitting layer was prepared under an N_2 atmosphere and spin-coated (at 2000 rpm) on the PEDOT:PSS layer with a thickness of 50 nm. The TmPyPB layer (45 nm) was thermally deposited onto the emitting layer. Finally, a thin layer (1 nm) of LiF followed by Al capping layer (100 nm) was deposited onto the substrate under vacuum (5´10^{-6} Pa). Current density-voltage (*J*-*V*) characteristics were collected using a Keithley 2400 source meter equipped with a calibrated silicon photodiode. The NIR EL irradiance (*R*) was measured through a PR735 SpectraScan spectrometer. The external quantum efficiency (η_{EQE}) of the NIR emission was obtained by measuring the irradiance in the forward direction and assuming the external emission profile to Lambertian.

References

1 J. H. Palmer, A. C. Durrell, Z. Gross, J. R. Winkler and H. B. Gray, *J. Am. Chem. Soc.*, 2010, **132**, 9230-9231.

2 G. R. Fu, H. Zheng, Y. N. He, W. T. Li, X. Q. Lü and H. S. He, *J. Mater. Chem. C*, 2018, **6**, 10589-10596.

3 S. Kesarkar, W. Mróz, M. Penconi, M. Pasini, S. Destri, M. Cazzaniga, D. Ceresoli, P. R. Mussini, C. Baldoli, U. Giovanella and A. Bossi, *Angew. Chem. Int. Ed.*, 2016, **55**, 2714-2718

4 G. M. Sheldrick, *SHELXL-97*, *Program for Crystal Structure Refinement*, University of 12 Göttingen, Göttingen, Germany, 1997.

5 G. M. Sheldrick, G. M. *SADABS*, University of Göttingen, Göttingen, Germany, 1996.

6 W. R. Wadt and P. J. Hay, *J. Chem. Phys.,* 1985, **82**, 284-298.

7 P. J. Hay and W. R. Wadt, *J. Chem. Phys.*, 1985, **82**, 299-310.

8 T. Lu, Multiwfn Manual, version 3.6 (dev), Section 3.21.1 and 3.21.8, available at http://sobereva.com/multiwfn.

9 P. Ros and G. C. A. Schuit, *Theor. Chim. Acta.,* 1966, **4**, 44-63.

10 T. Lu and F. W. Chen, *J. Comput. Chem.* 2012, **33**, 580-592.

11 M. J. Frisch, G. W. Trucks, H. B. Schlegel, G. E. Scuseria, M. A. Robb, J. R. Cheeseman, G. Scalmani, V. Barone, B. Mennucci, G. A. Petersson, H. Nakatsuji, M. Caricato, X. Li, H. P. Hratchian, A. F. Izmaylov, J. Bloino, G. Zheng, J. L. Sonnenberg, M. Hada, M. Ehara, K. Toyota, R. Fukuda, J. Hasegawa, M. Ishida, T. Nakajima, Y. Honda, O. Kitao, H. Nakai, T. Vreven, J. A. Montgomery, Jr., J. E. Peralta, F. Ogliaro, M. Bearpark, J. J. Heyd, E. Brothers, K. N. Kudin, V. N. Staroverov, R. Kobayashi, J. Normand, K. Raghavachari, A. Rendell, J. C. Burant, S. S. Iyengar, J. Tomasi, M. Cossi, N. Rega, J. M. Millam, M. Klene, J. E. Knox, J. B. Cross, V. Bakken, C. Adamo, J. Jaramillo, R. Gomperts, R. E. Stratmann, O. Yazyev, A. J. Austin, R. Cammi, C. Pomelli, J. W. Ochterski, R. L. Martin, K. Morokuma, V. G. Zakrzewski, G. A. Voth, P. Salvador, J. J. Dannenberg, S. Dapprich, A. D. Daniels, Ö. Farkas, J. B. Foresman, J. V. Ortiz, J. Cioslowski and D. J. Fox, Gaussian 09, Revision D.01, Gaussian, Inc., Wallingford CT, 2009.

12 X. B. Xu, X. L. Yang, Y. Wu, G. J. Zhou, C. Wu, and W.-Y. Wong, *Chem. Asian J.,* 2015, **10**, 252-262.

13 E. Zysman-Colman, S. S. Ghosh, G. Xie, S. Varghese, M. Chowdhury, N. Sharma, D. B. Cordes, A. M. Z. Slawin and I. D. W. Samuel, *ACS Appl. Mater. & Interfaces,* 2016, **8**, 9247-9253.

Table S1 Crystal data and structure refinement for the C_1-symmetric Ir(III)-complex [Ir(iqbt)(ppy)(pic)] (**1**) and [Ir(iqbt)(ppy)(Br-pic)]·2$CHCl_3$ (**2**·2$CHCl_3$)

Compound	**1**	**2**·2$CHCl_3$
Empirical formula	$C_{34}H_{22}N_3O_2SIr$	$C_{36}H_{23}N_3BrCl_6O_2SIr$
Formula weight	728.81	1046.44
Crystal system	monoclinic	monoclinic
Space group	$P2_1/n$	$P2_1/c$
a/Å	11.7447(12)	12.768(4)
b/Å	8.8623(9)	17.123(5)
c/Å	28.170(3)	16.962(5)
α/°	90	90
β/°	91.674(2)	96.444(5)
γ/°	90	90
V/Å^3	2930.9(5)	3684.7(19)
Z	4	4
ρ/g·cm^{-3}	1.652	1.886
Crystal size/mm	0.22× 0.20× 0.16	0.24× 0.22× 0.18
μ(Mo-Kα)/mm^{-1}	4.662	5.238
Data/restraints/parameters	5800/0/370	7369 /0 /451
Quality-of-fit indicator	1.044	1.052
No. unique reflections	5800	7369
No. observed reflections	15252	19998
Final R indices [I> 2σ(I)]	R_1 = 0.0472	R_1 = 0.0402
	wR_2 = 0.1520	wR_2 = 0.1064
R indices (all data)	R_1 = 0.0602	R_1 = 0.0632
	wR_2 = 0.1601	wR_2 = 0.1338

Table S2 The relevant bond lengths (Å) and bond angles (°) for the C_1-symmetric Ir(III)-complex [Ir(iqbt)(ppy)(pic)] (**1**) and [Ir(iqbt)(ppy)(Br-pic)] ·2$CHCl_3$ (**2**·2$CHCl_3$)

Compound	**1**	**2**·2$CHCl_3$
Ir(1)-C(11)	1.994(9)	1.991(7)
Ir(1)-N(1)	2.032(7)	2.018(6)
Ir(1)-N(3)	2.138(7)	2.153(6)
Ir(1)-C(18)	2.000(9)	2.006(8)
Ir(1)-N(2)	2.050(7)	2.041(6)
Ir(1)-O(1)	2.172(6)	2.168(5
C(11)-Ir(1)-C(18)	89.7(3)	86.6(3)
C(11)-Ir(1)-N(2)	101.1(3)	101.5(3)
C(11)-Ir(1)-N(3)	97.5(3)	99.6(2)
C(11)-Ir(1)-N(1)	79.4(3)	79.0(2)
C(11)-Ir(1)-O(1)	171.6(3)	172.5(2)

Table S3 The photophysical properties of the C_1-symmetric [Ir(C^N^1)(C^N^2)(N^O)-*tris*-heteroleptic Ir(III)-complexes [Ir(iqbt)(ppy)(pic)] (**1**) and [Ir(iqbt)(ppy)(Br-pic)] (**2**) in degassed CH_2Cl_2 solution at room temperature (RT) or 77 K

Comp.	Absorption[a]	Emission[a] (RT)						Emission[a] (77 K)	
	λ_{abs} [nm]	λ_{em} [nm]	S_M[c]	τ [μs]	Φ_{PL}	k_r[b] (10^5 s^{-1})	k_{nr}[b] (10^6 s^{-1})	λ_{em} [nm]	S_M[c]
1	226, 263, 311, 456, 518	699, 760(sh)	0.31	0.34	0.27	7.9	2.1	698, 764(sh)	0.28
2	226, 261, 323, 368, 454, 516	697, 754(sh)	0.31	0.35	0.21	2.3	2.1	696, 760(sh)	0.30

[a]Measured in degassed CH_2Cl_2 solution;

[b]$k_r = \Phi_{PL}/\tau$, $k_{nr} = (1 - \Phi_{PL})/\tau$;

[c]Huang–Rhys factor (S_M) is calculated from the peak heights and energies of (0−0) and (0−1) band, $S_M = (I_{0-1}/I_{0-0})$ ($\bar{\nu}_{0\text{-}0}/\ \bar{\nu}_{0\text{-}1}$).

Table S4 The DFT/TD-DFT calculation results of the Ir(III)-complexes [Ir(iqbt)(ppy)(pic)] (**1**) and [Ir(iqbt)(ppy)(Br-pic)] (**2**) on the basis of their optimized S_0 geometries

Complex	MO	Contribution of metal d_π orbitals and π orbitals of ligand to MOs (%)				Main configuration of $S_0 \rightarrow S_n$ excitation, λ_{cal} (nm)/f[a]	Main configuration of $S_0 \rightarrow T_1$ excitation, λ_{cal} (nm)[b]
		Ir	iqbt	ppy	L(N^O)		
1	LUMO+2	4.43	0.27	87.55	7.75	$S_0 \rightarrow S_1$: H → L (94.98%), 519, 0.0934	H-1 → L (8.36%),
	LUMO+1	2.07	0.76	7.79	89.39		
	LUMO	5.16	92.69	0.37	1.78	$S_0 \rightarrow S_2$: H → L+1 (98.14%), 455, 0.0033	H →L (86.67%),
	HOMO	28.62	53.24	15.04	3.11	$S_0 \rightarrow S_3$: H → L+2 (96.30%), 440, 0.0112	697
	HOMO-1	8.21	43.05	45.64	3.09		
	HOMO-2	51.82	7.32	13.42	27.44		
2	LUMO+2	4.32	0.31	93.04	2.33	$S_0 \rightarrow S_1$: H → L (94.69%), 517, 0.0941	H-1 → L (8.22%),
	LUMO+1	2.36	1.58	1.58	94.49		
	LUMO	4.99	91.70	0.38	2.92	$S_0 \rightarrow S_2$: H → L+1 (98.24%), 479, 0.0028	H → L (86.05%),
	HOMO	28.05	54.18	14.84	2.94	$S_0 \rightarrow S_3$: H → L+2 (96.66%), 439, 0.0116	695
	HOMO-1	8.33	42.26	46.65	2.76		
	HOMO-2	52.00	7.78	15.05	25.18		

[a]H → L denotes the transition from HOMO to LUMO. λ_{cal}, and f denote the calculated emission wavelength, and oscillator strength, respectively. The oscillator strength of $S_0 \rightarrow T_1$ is zero owing to the spin-forbidden character of the singlet-triplet transition under TD-DFT calculations in the Gaussian program with no consideration of spin orbital coupling.

Table S5 The TD-DFT calculation results of the Ir(III)-complexes [Ir(iqbt)(ppy)(pic)] (**1**) and [Ir(iqbt)(ppy)(Br-pic)] (**2**) on the basis of their optimized T_1 geometries

Complex	MO	Contribution of metal d_π orbitals and π orbitals of ligand to MOs (%)				Main configuration of $T_1 \rightarrow S_0$ emission, λ_{cal} (nm)[b]
		Ir	iqbt	ppy	L(N^O)	
1	LUMO+1	1.90	0.54	10.36	87.20	H → L (95.3%), H-1 → L (5.4%), 916
	LUMO	6.35	91.35	0.64	1.66	
	HOMO	22.20	66.42	9.06	2.32	
	HOMO-1	14.23	36.39	45.01	4.37	
2	LUMO+1	1.98	0.53	1.23	96.26	H → L (93.4%), H -1 → L (5.2%), 917
	LUMO	6.32	91.06	0.73	1.89	
	HOMO	21.75	67.17	8.85	2.22	
	HOMO-1	14.25	35.73	46.00	4.02	

[a]H → L denotes the transition from HOMO to LUMO. λ_{cal}, and f denote the calculated emission wavelength, and oscillator strength, respectively. The oscillator strength of $T_1 \rightarrow S_0$ is zero owing to the spin-forbidden character of the singlet-triplet transition under TD-DFT calculations in the Gaussian program with no consideration of spin-orbital coupling.

Table S6 Interfragment charge transfer (IFCT) analysis for the Ir(III)-complexes [Ir(iqbt)(ppy)(pic)] (**1**) and [Ir(iqbt)(ppy)(Br-pic)] (**2**) by TD-DFT calculations with the IFCT analyses at the B3LYP level

complex	state	*λ* (nm)	*E* (eV)	Oscillator (*f*)	transition (contrib.)	Assignment (%)			
1	$S_0 \rightarrow S_1$	519	2.3878	0.0934	HOMO → LUMO (95.0%),	^{1}LC	34.99	^{1}MC	2.293
						^{1}MLCT	36.602	^{1}LMCT	3.601
						^{1}LLCT	22.514		
	$S_0 \rightarrow T_1$	697	2.7789	0.0000	HOMO → LUMO (86.7%), HOMO-1 → LUMO (8.4%),	^{3}LC	70.726	^{3}MC	1.084
						^{3}MLCT	17.107	^{3}LMCT	4.875
						^{3}LLCT	6.207		
	$T_1 \rightarrow S_0$	916	1.3539	0.0000	HOMO → LUMO (95.3%), HOMO-1 → LUMO (5.4%),	^{3}LC	75.120	^{1}MC	0.992
						^{3}MLCT	20.24	^{3}LLCT	4.641
2	$S_0 \rightarrow S_1$	517	2.4003	0.0941	HOMO → LUMO (94.7%),	^{1}LC	35.468	^{1}MC	2.232
						^{1}MLCT	36.195	^{1}LMCT	3.577
						^{1}LLCT	22.529		
	$S_0 \rightarrow T_1$	695	1.7843	0.0000	HOMO → LUMO (86.1%), HOMO-1 → LUMO (8.2%);	^{3}LC	71.471	^{3}MC	1.050
						^{3}MLCT	16.631	^{3}LMCT	4.889
						^{3}LLCT	5.958		
	$T_1 \rightarrow S_0$	917	1.3525	0.0000	HOMO → LUMO (93.4%), HOMO -1 → LUMO (5.2%);	^{3}LC	75.326	^{3}MC	0.971
						^{3}MLCT	19.93	^{3}LLCT	4.728

Table S7 The transition dipole moment (TDM) vectors $\vec{\mu}$-S_0, $\vec{\mu}$-T_1 and $\vec{\mu}$-($T_1 \rightarrow S_0$) for the C_1-symmetric [Ir(C^N^1)(C^N^2)(N^O)-*tris*-heteroleptic Ir(III)-complexes [Ir(iqbt)(ppy)(pic)] (**1**) and [Ir(iqbt)(ppy)(Br-pic)] (**2**) upon DFT calculations based on their corresponding optimized T_1 and S_0 states

Complex	State	*x*	*y*	*z*	$\lvert\vec{\mu}\rvert$ (D)	θ (°)	$\lvert\vec{\mu}\rvert$ (^{1}T-^{0}S) (D)
1	S_0	-1.0935	2.6268	-5.0210	5.77	22	2.24
	T_1	1.1181	2.9052	-4.8904	5.80		
2	S_0	-0.5710	1.0887	5.2075	5.35	22	2.12
	T_1	-1.2141	-0.9418	5.3185	5.54		

Table S8. Summarized coefficients (maximum ordinary coefficient k_o^{max}, maximum extraordinary coefficient k_e^{max}), θ' angles between the transition dipole moment vector and the direction vertical to the substrate, order parameters (*S*), and horizontal dipole ratios ($h/(h+v)$) of the spin-coated EMLs for the **NIR-PELDs-1-2** composed of PVK-OXD7 (65:30, wt%) as the host and each of the Ir(III)-complexes **1**-**2** as the dopant at 5 wt% doping level.

EML	k_e^{max} (λ)	k_o^{max} (λ)	θ' (°)	S[a]	$h/(h+v)$[b]
PVK:OXD7:**1** (65:30:5; wt%)	0.636 (233 nm)	0.854 (235 nm)	58.61	-0.093	73.0%
PVK:OXD7:**2** (65:30:5; wt%)	0.529 (235 nm)	0.604 (233 nm)	55.51	-0.043	69.5%

$$S = \frac{k_e^{max} - k_o^{max}}{k_e^{max} + 2k_o^{max}} = \frac{3cos^2\theta' - 1}{2} \quad (4)$$

[a]

$$\frac{h}{h+v} = \frac{2(1-S)}{3} \quad (5)$$

[b]

Figure S1 The ^{1}H NMR spectra of the C^N^{1} main ligand **Hiqbt**, the [Ir(C^N)$_2$(N^O)]-*bis*-heteroleptic Ir(III)-complex **[Ir(iqbt)$_2$(Br-pic)]**, and the [Ir(C^N^{1})(C^N^{2})(N^O)]-*tris*-heteroleptic Ir(III)-complexes [Ir(iqbt)(ppy)(pic)] (**1**) and [Ir(iqbt)(ppy)(Br-pic)] (**2**) in $CDCl_3$ and/or DMSO-d_6 at room temperature.

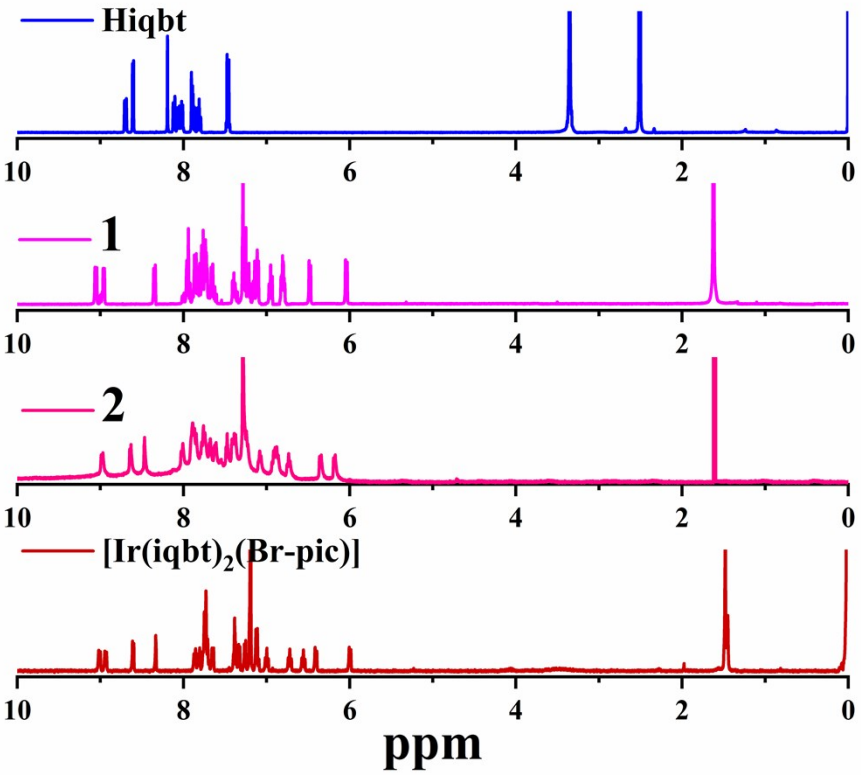

Figure S2 The ^{13}C NMR spectra of the [Ir(C^N^1)(C^N^2)(N^O)]-*tris*-heteroleptic Ir(III)-complexes [Ir(iqbt)(ppy)(pic)] (**1**) and [Ir(iqbt)(ppy)(Br-pic)] (**2**) in $CDCl_3$ at room temperature.

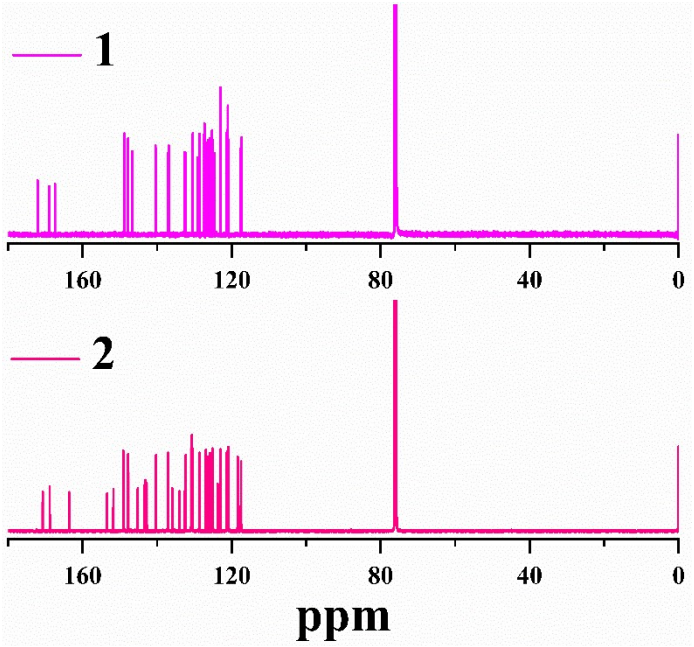

Figure S3 The ESI-MS results of the [Ir(C^N^1)(C^N^2)(N^O)]-*tris*-heteroleptic Ir(III)-complexes [Ir(iqbt)(ppy)(pic)] (**1**) and [Ir(iqbt)(ppy)(Br-pic)] (**2**) in CH_2Cl_2.

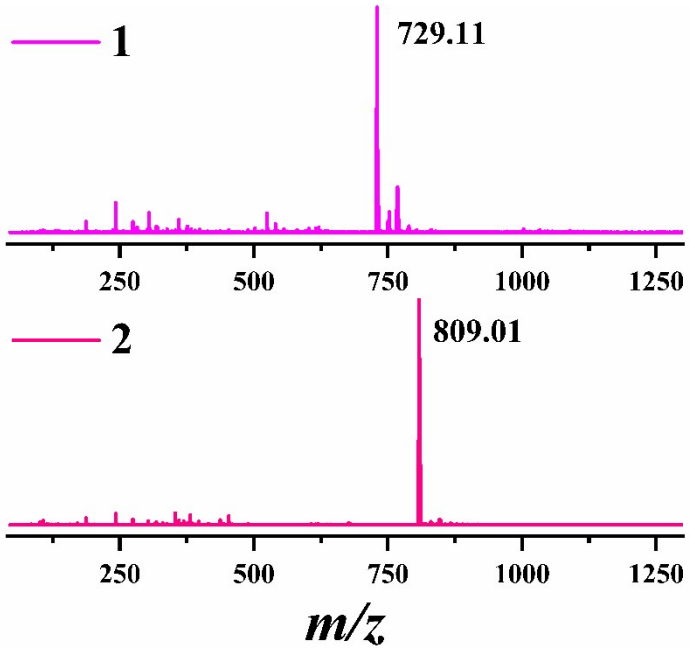

Figure S4 The TG (thermogravimetric) curves for the C_1-symmetric [Ir(C^N^1)(C^N^2)(N^O)]-*tris*-heteroleptic Ir(III)-complexes [Ir(iqbt)(ppy)(pic)] (**1**) and [Ir(iqbt)(ppy)(Br-pic)] (**2**).

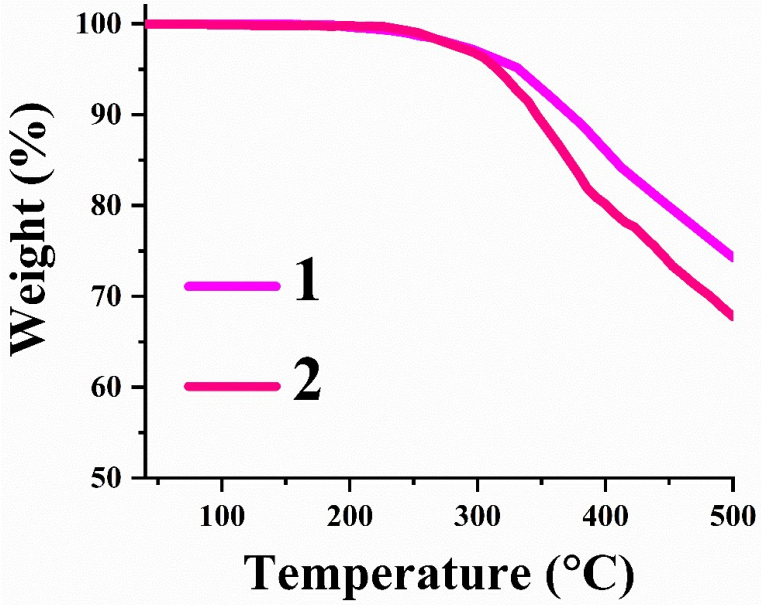

Figure S5 The normalized UV-visible absorption of the ligands **Hiqbt, Hppy, Hpic** and **Br-Hpic** in degassed CH_2Cl_2 solution at room temperature.

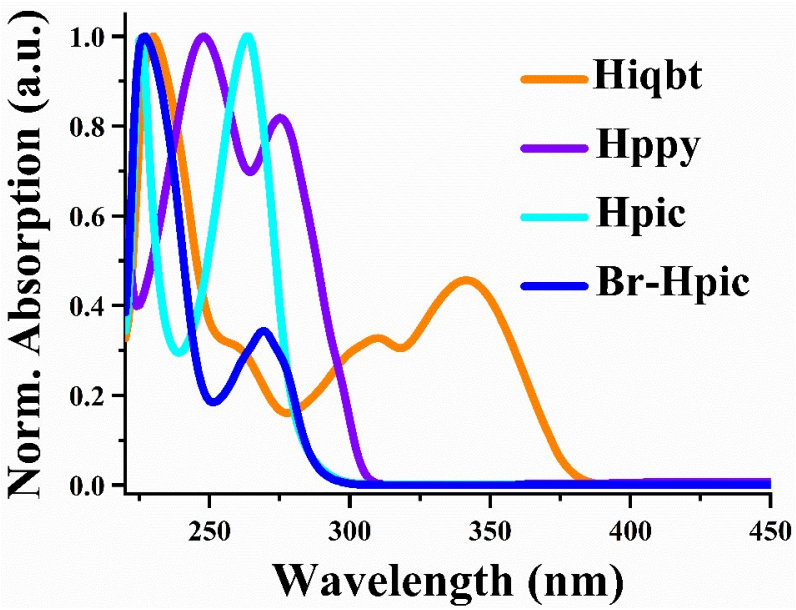

Figure S6 The normalized UV-visible absorption of the four by-products (**[Ir(iqbt)$_2$(pic)]**, **[Ir(ppy)$_2$(pic)]**, **[Ir(iqbt)$_2$(Br-pic)]** and **[Ir(ppy)$_2$(Br-pic)]**) in degassed CH_2Cl_2 solution at room temperature.

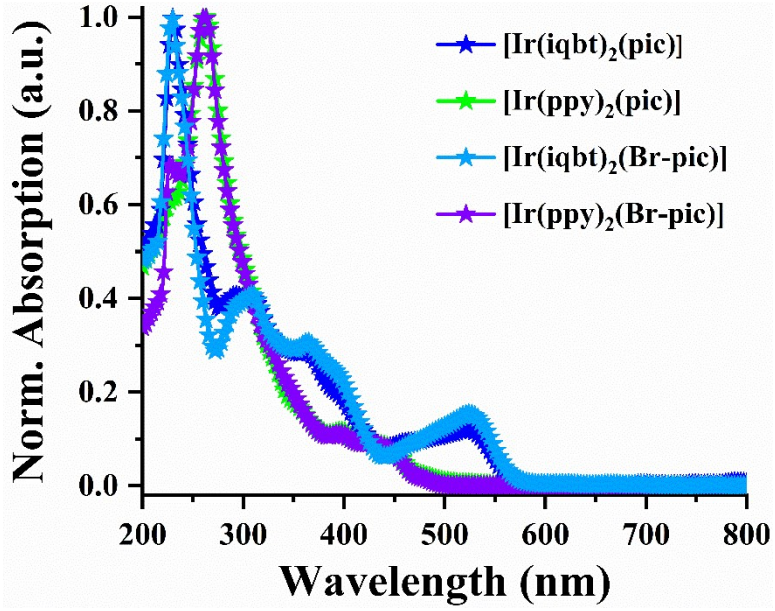

Figure S7 The normalized emission spectra of the ligands **Hiqbt, Hppy, Hpic** and **Br-Hpic** in degassed CH_2Cl_2 solution at room temperature.

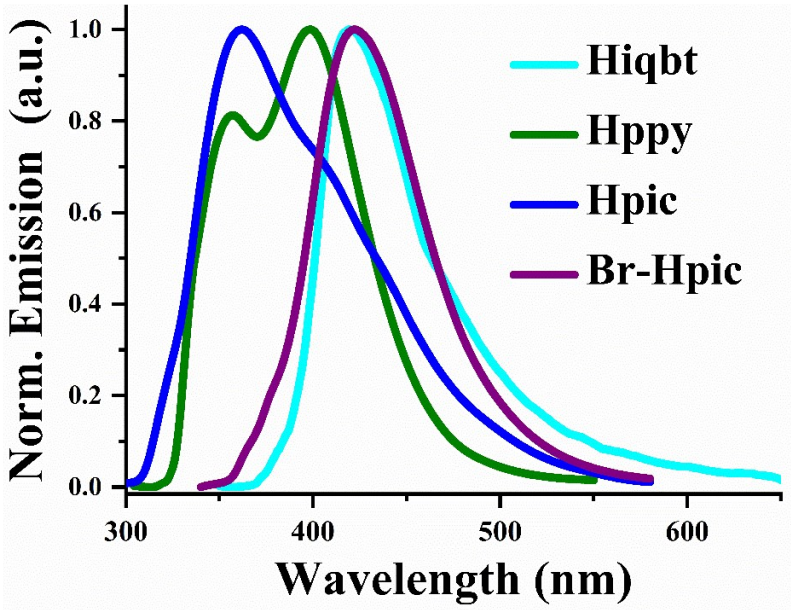

Figure S8 The normalized emission spectra of the four by-products (**[Ir(iqbt)$_2$(pic)]**, **[Ir(ppy)$_2$(pic)]**, **[Ir(iqbt)$_2$(Br-pic)]** and **[Ir(ppy)$_2$(Br-pic)]**) in degassed CH_2Cl_2 solution at room temperature.

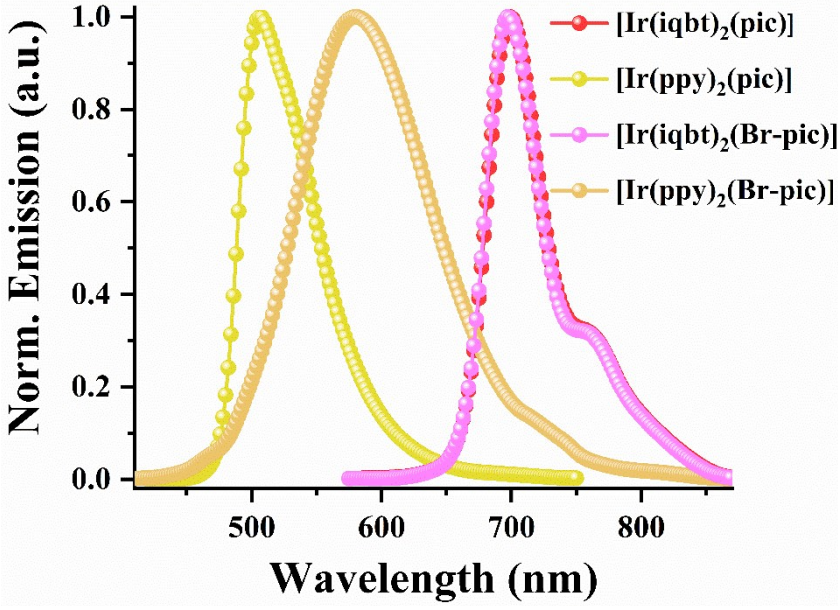

Figure S9 The CV (cyclic voltammogram) curves of for the C_1-symmetric [Ir(C^N^1)(C^N^2)(N^O)]-*tris*-heteroleptic Ir(III)-complexes [Ir(iqbt)(ppy)(pic)] (**1**) and [Ir(iqbt)(ppy)(Br-pic)] (**2**)

recorded *versus* Fc^+/Fc in degassed MeCN solution at room temperature under a N_2 atmosphere (scan rate = 100 mV/s).